Propagation of quantized fields through negative-index media

Martin Ligare[*]

Department of Physics & Astronomy, Bucknell University, Lewisburg, PA 17837
(*Received 00 Month 200x; final version received 00 Month 200x*)

Dielectric materials in which both the relative permittivity, ϵ, and the relative permeability, μ, are negative exhibit striking optical properties, which are the consequence of the fact that the effective index of refraction in such materials is negative. Most studies of the propagation of electromagnetic fields in these media have concentrated on classical fields with well-defined phases. In contrast, I use simple fully-quantized models to illustrate how some of the striking properties of negative-index media are manifested in the propagation of single, spontaneously emitted, photons. Single-photon quantum fields do not have an absolute phase, but the examples in this paper demonstrate a quantum analog of the negative phase accumulated by classical fields as photons propagate through negative-index media. The single photons also exhibit classical reflection and transmission coefficients, as well as the expected group velocity.

1.   Introduction

Dielectric materials in which the relative permittivity, ϵ, and the relative permeability, μ, are both negative exhibit striking optical properties, which are the consequence of the fact that the effective index of refraction in such materials is negative. Such materials were first the subject of systematic theoretical investigation in 1967 [1], and recent advances in the fabrication of such negative-index metamaterials have led to a resurgence of research in this area. Proposals for exciting applications of negative-index media, such as so-called perfect lenses [2], have contributed to the continuing interest in these materials.The history and state of the field have been summarized in several review articles [3–6] and books [7, 8].

In this paper I investigate simple idealized models of a quantized single-photon field propagating through a negative-index medium and across vacuum-dielectric interfaces. Most investigations of the propagation of electromagnetic radiation in negative-index media have concentrated on classical fields. The classical description of electromagnetic fields is clearly adequate for most practical applications of negative-index media proposed to date, but it is still instructive to consider the striking properties of negative-index media in the context of a quantized theory.

One of the striking features of classical waves in negative-index media is a phase velocity that is directed opposite to the direction of the energy flow. In a quantum field theory the concept of the phase of a field is not as clear as it is in classical physics, and the way in which a negative phase velocity might be manifested is not obvious. The phase of a quantized field has been the subject of investigation from the early days of quantum mechanics [9, 10]. Most previous work on the phase of a quantum field has focused on defining a meaningful and mathematically well-behaved phase operator for *single-mode* fields; the states with well-defined phases are linear combinations of states of the single-mode with different occupation numbers. In contrast to those treatments, I investigate commonly encountered *single-photon* fields, specifically those that result from spontaneous emission of an excited atom. The states describing these fields are linear combinations of many different modes of the field, but all of the modes are singly occupied.

---

[*]Email: mligare@bucknell.edu
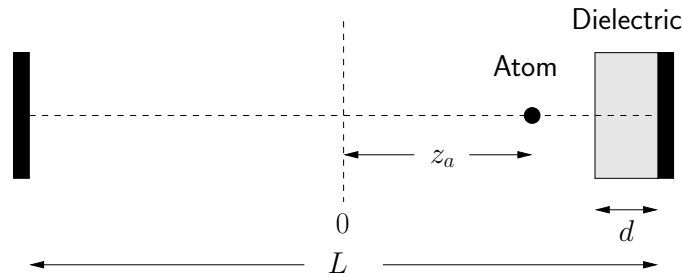
Figure 1. One-dimensional model for investigation of propagation of quantized fields through negative-index media. A single two-level atom spontaneously emits a photon into a large multimode optical cavity with a thin region of dispersive dielectric material at one end.

I address the question "How can a negative phase velocity be detected in the propagation of a single photon, a quantum object that does not have a definite phase?"

The models I use show explicitly how the characteristics of classical fields are manifested in the propagation of single photons, and highlight the connections between quantum and classical models of propagation. I also illustrate the classical-like properties of single-photon fields that are reflected at the interface between a vacuum and a negative-index material. The examples in this paper will be restricted to one-dimensional models with a single polarization; two-dimensional models that illustrate refraction will be investigated in a future study.

The material properties and the idealized models considered in this paper are not chosen to correspond to realistic materials or specific experiments. They are, rather, chosen to illustrate fundamental correspondences between quantum and classical fields. In order to highlight these correspondences I limit consideration to materials and frequencies for which the properties ϵ and μ can be treated as isotropic and macroscopic, and for which absorption can be considered negligible in the frequency range of the emitted radiation [11]. This is a significant simplification, and absorption must play a role in the description of any realistic negative-index device. The focus of this paper, however, is not the details of the field quantization scheme; rather, it is the identification of classical negative phase effects in the context of the simplest possible quantized single-photon theory. It is hoped that future studies with more a more realisitic treatment of the aborbing medium may lead to additional insight.

An example of the simple models explored in this paper is illustrated in Fig. 1. This figure shows a one-dimensional "universe" of length L with perfectly reflecting mirrors as boundaries, and a region of dispersive dielectric material situated at the right end. An excited two-level atom is located to the left of the dielectric slab, and serves as a source of a single-photon field. The propagation of the emitted field is tracked in two ways: first in the evolution of the expectation value of the field intensity (as a function of position and time) as the pulse propagates away from the atom, through the dielectric, and eventually reflects off of the end wall and returns to the vacuum region, and second, by the effect of the field on the emitting atom when it returns. The length L is assumed to be very much greater than the resonant wavelength of the atom, and the spectrum of the emitted radiation spans very many modes of the cavity.

The relevant properties of classical fields in negative-index media are reviewed in Section 2. In making the transition from a classical to a quantum mechanical treatment of the radiation field in in Section 3, I quantize the standing-wave modes of the entire volume containing both the vacuum regions and the dielectric material. Although this quantization scheme is based on standing-wave modes, this technique has been demonstrated to be useful in previous studies of propagating photons when many modes are included in the calculation of the dynamics of the system [12–17]. This approach is well suited to investigations of anomalous light propagation because it highlights the time dependence of optical systems, illustrating clearly the causal evolution of single-photon wavefronts. It is especially illuminating for investigation of propagation in negative index-media because it reveals the quantum analogs of classical phase effects [14–

16]. Formal expressions for the time-dependent quantum variables of interest are developed in Section 4, and the principal results are presented in the graphs of Section 5, which illustrate the evolving expectation value of the field intensity as the light propagates, as well time-dependent amplitudes for atomic excitation.

2. Summary of Classical Results

Within a negative-index medium, Maxwell's equations have the same form they do in vacuum, because the dielectric properties only enter as the product $\epsilon\mu$. This leads to the usual monochromatic traveling wave solutions

$$\mathbf{E}_{\text{tr}} = \mathbf{E}_0 e^{i(\mathbf{k}\cdot\mathbf{r}-\omega t)} \tag{1}$$

$$\mathbf{B}_{\text{tr}} = \frac{\sqrt{\epsilon\mu}}{c} E_0 e^{i(\mathbf{k}\cdot\mathbf{r}-\omega t)} \left(\hat{\mathbf{k}} \times \hat{\mathbf{E}}_{\mathbf{0}}\right) \tag{2}$$

as well as standing wave solutions of the familiar form

$$\mathbf{E}_{\text{sw}} = \mathbf{E}_0 \cos(\mathbf{k}\cdot\mathbf{r}+\alpha)\cos(\omega t) \tag{3}$$

$$\mathbf{B}_{\text{sw}} = \frac{\sqrt{\epsilon\mu}}{c} E_0 \sin(\mathbf{k}\cdot\mathbf{r}+\alpha)\cos(\omega t) \left(\hat{\mathbf{k}} \times \hat{\mathbf{E}}_{\mathbf{0}}\right). \tag{4}$$

In these equations, and throughout this paper, the quantity $\sqrt{\epsilon\mu}$ refers to the positive square root. The trio of vectors $\mathbf{E}_{\text{tr}}$, $\mathbf{B}_{\text{tr}}$, and $\mathbf{k}$ are mutually perpendicular, with the same "right-handed" relationship as in normal media. (The trio of vectors $\mathbf{E}_{\text{tr}}$, $\mathbf{H}_{\text{tr}}$, and $\mathbf{k}$ have a "left-handed" relationship.) The energy flux density is given by the Poynting vector

$$\mathbf{S} = \frac{c}{4\pi}\left(\mathbf{E}\times\mathbf{H}\right) = \frac{c}{4\pi\mu}\left(\mathbf{E}\times\mathbf{B}\right), \tag{5}$$

which means that in negative-index media the wave-vector $\mathbf{k}$ (oriented in the direction of $\mathbf{E}\times\mathbf{B}$) is anti-parallel to the Poynting vector $\mathbf{S}$, i.e., the direction of the phase velocity is opposite to the direction of the energy flow. One consequence is that in a negative-index medium the optical path length for a wave propagating a distance d is $-\sqrt{\mu\epsilon}\,d$, which means that the wave is accumulating negative phase as it propagates.

The group velocity is given by the usual expression

$$v_{\text{gr}} = \frac{d\omega}{dk} = \frac{c}{\sqrt{\epsilon\mu} + \frac{1}{2}\frac{\omega}{\sqrt{\epsilon\mu}}\left(\mu\frac{d\epsilon}{d\omega} + \epsilon\frac{d\mu}{d\omega}\right)}, \tag{6}$$

and the approximate energy density in a transparency window is [11]

$$\overline{U} = \frac{1}{8\pi}\left[\frac{d(\omega\epsilon)}{d\omega}\overline{E^2} + \frac{d(\omega\mu)}{d\omega}\overline{H^2}\right]. \tag{7}$$

The derivatives $d(\omega\epsilon)/d\omega$ and $d(\omega\mu)/d\omega$ must be positive in any dispersive medium and these conditions ensure that the energy density is positive. These conditions also imply that the group velocity, given by Eq. (6), will be negative whenever ϵ and μ are both negative. This means that the direction of pulse propagation is opposite to the direction of the wave vector $\mathbf{k}$, or equivalently, in the direction of $\mathbf{S}$. For transparent media like those considered in this paper

4   *M. Ligare*

stronger conditions apply [11]: $d\epsilon/d\omega > 2(1-\epsilon)/\omega$ and $d\mu/d\omega > 2(1-\mu)/\omega$. These conditions guarantee that the wave speeds satisfy the condition

$$|v_{\mathrm{gr}}| < \frac{c}{\left(\sqrt{\epsilon\mu} + \sqrt{\frac{\epsilon}{\mu}} + \sqrt{\frac{\mu}{\epsilon}}\right)} < |v_{\mathrm{ph}}|. \tag{8}$$

3. Field Quantization

The field quantization scheme used in this paper is similar in spirit to the phenomenological quantization in negative-index media discussed by Milonni and Maclay [18], which builds on the earlier work of Milonni treating field quantization in non-absorbing dispersive dielectrics [19]. In contrast to the scheme used by Milonni and Maclay, I quantize standing-wave modes rather than traveling-wave modes. I also use modes of the entire volume that includes the vacuum and dielectric region, in a manner similar to the scheme that is discussed in previous treatments of quantization in inhomogeneous, lossless, linear dielectrics [20–22]. Field quantization and spontaneous emission of atoms in negative-index media have also been discussed in [23] and [24]. It should also be noted that more realistic quantization schemes for lossy dielectrics have been a subject of considerable interest (see, for example, [25–27]).

For a one-dimensional system like that illustrated in Fig. 1, the classical field can be expanded in a complete set of spatial modes $\mathcal{E}_m(z)$ as

$$E(z,t) = \sum_m a_m(t)\mathcal{E}_m(z), \tag{9}$$

where the spatial mode functions satisfy the equation

$$\frac{d^2\mathcal{E}_m}{dz^2} + \frac{1}{\epsilon(\omega_m,z)\mu(\omega_m,z)}\mathcal{E}_m = 0, \tag{10}$$

and the permittivity ϵ and permeability μ are both functions of position and mode frequency.

The models considered in this paper are comprised of regions in which ϵ and μ are constant in space, and the product $\epsilon\mu$ is positive (with either ϵ and μ both positive, or both negative). Within each region the mode functions are therefore sinusoidal, with the form of Eqs. (3) & (4). It is a straightforward boundary-value problem to find the vacuum wave numbers, k_m^{vac}, and the corresponding mode frequencies, $\omega_m = ck_m^{\mathrm{vac}}$, as well as the complete spatial mode functions, $\mathcal{E}_m(z)$; an outline of a typical calculation is given in the Appendix.

The resulting mode frequencies and mode functions depend on the functional dependence of ϵ and μ on the frequency ω. In this paper I use a simple model in which I assume that the range of relevant frequencies is small enough that the dispersion in both ϵ and μ can be assumed to be linear, i.e.,

$$\epsilon(\omega) = \epsilon(\omega_0) + \frac{d\epsilon}{d\omega}(\omega - \omega_0) \tag{11}$$

$$\mu(\omega) = \mu(\omega_0) + \frac{d\mu}{d\omega}(\omega - \omega_0). \tag{12}$$

The values of the constants characterizing the dielectric media that are used in the examples in this paper are given in Table 1.

The classical coefficients $a_m(t)$ in the linear combination of modes given by Eq. (9) obey the equation of motion of a harmonic oscillator, and the field is quantized in the standard way by

Table 1.   Material constants used in calculations along with resulting classical wave speeds.

Section	$\epsilon(\omega_0)$	$\omega_0\, d\epsilon/d\omega$	$\mu(\omega_0)$	$\omega_0\, d\mu/d\omega$	$\sqrt{\mu(\omega_0)\epsilon(\omega_0)}$	$|v_{\mathrm{ph}}|$	$|v_{\mathrm{gr}}|$
5.1	$-\frac{3}{2}$	$\frac{25}{4}$	$-\frac{3}{2}$	$\frac{25}{4}$	$\frac{3}{2}$	$\frac{2}{3}c$	$\frac{4}{19}c$
5.2	-3	$\frac{48}{5}$	$-\frac{4}{3}$	$\frac{28}{5}$	2	$\frac{1}{2}c$	$\frac{5}{27}c$

promoting the coefficients to operators. The mode functions are normalized so that the integral of the energy density over the quantization volume gives $\hbar\omega_m$, and the electric field operator becomes

$$\hat{E}(z) = \sum_m \mathcal{E}_m(z)\left(a_m + a_m^\dagger\right), \tag{13}$$

where the functions $\mathcal{E}_m(z)$ are the classical mode functions and $a_m^\dagger$ and a_m are the raising and lowering operators for each quantized mode of the field. The free-field Hamiltonian is

$$H_{\mathrm{field}} = \sum_m \hbar\omega_n\left(a_m^\dagger a_m + \frac{1}{2}\right). \tag{14}$$

The fact that I am treating a negative-index medium does not enter this quantization scheme in a prominent way, and the standing-wave mode functions have the same sinusoidal form as the mode functions for positive-index media in each of the regions. The only place where the negative-index character enters is in the boundary condition for the magnetic field at the vacuum-dielectric interfaces. This boundary condition is crucial, however, in the determination of the mode functions and frequencies.

4.   Quantum Dynamics

In this section I introduce the standard interaction Hamiltonian that I use, and present formal results for the time dependence of the system. The model system illustrated in Fig. 1 consists of a single two-level atom, with zero-field resonant frequency ω_a and electric dipole matrix element d, and the atom is located at a fixed positions z_a. The atomic plus free-field Hamiltonian is

$$\begin{aligned}\hat{H}_0 &= \hat{H}_{\mathrm{atom}} + \hat{H}_{\mathrm{field}} \\ &= \hbar\omega_a\sigma^z + \sum_m \hbar\omega_m a_m^\dagger a_m,\end{aligned} \tag{15}$$

where σ^z is the third component of the atomic pseudo-spin operator of the atom. (I have re-zeroed the energy scale to remove the zero-point energies of the field modes.) The basis states are the eigenstates of H_0 and are denoted as follows:

- $|e;0\rangle$ — atom excited; no photons in field,
- $|g;1_m\rangle$ — atom in ground state; one photon in field mode with frequency ω_m.

I use the standard electric-dipole and rotating-wave approximations in the interaction Hamiltonian [28–30] to give

$$\begin{aligned}\hat{H} &= \hat{H}_0 + \hat{H}_{\mathrm{interaction}} \\ &= \hat{H}_{\mathrm{atom}} + \hat{H}_{\mathrm{field}} + \sum_m \hbar\left(g_m a_m \sigma^+ + g_m^* a_m^\dagger \sigma^-\right),\end{aligned} \tag{16}$$

M. Ligare

where σ^+ and σ^- act as raising and lowering operators for the atom, and the strength of the coupling of the atom to mode m is characterized by the constant g_m. The atom-field coupling strength g_m is a product of the atomic dipole moment and the field strength in the mode at the position of the atom:

$$g_m = d\mathcal{E}_m(z_a). \tag{17}$$

In what follows I work in the Schrödinger picture in which the time dependence is captured in the evolution of the state vector, and the operators are stationary. In the initial state, the source atom is in the excited state, and there are no photons in the field,i.e.,

$$|\psi(0)\rangle = |e;0\rangle. \tag{18}$$

The general state of the system at a later time is given by the linear combination

$$|\psi(t)\rangle = c(t)|e;0\rangle + \sum_m b_m(t)|g;1_m\rangle. \tag{19}$$

A formal expression for the time evolution of the system is obtained by projecting the initial state onto the energy eigenstates,

$$|\psi(0)\rangle = \sum_q |E_q\rangle\langle E_q|\psi(0)\rangle = \sum_q |E_q\rangle\langle E_q|e;0\rangle, \tag{20}$$

and then using the known time evolution of the eigenstates to give

$$|\psi(t)\rangle = \sum_q e^{-iE_q t/\hbar}|E_q\rangle\langle E_q|e;0\rangle. \tag{21}$$

Projecting $|\psi(t)\rangle$ back onto the basis states gives the coefficients in the linear combination of Eq. (19):

$$c(t) = \langle e;0|\psi(t)\rangle = \sum_q e^{-iE_q t/\hbar}\langle e;0|E_q\rangle\langle E_q|e;0\rangle, \tag{22a}$$

$$b_m(t) = \langle g;1_m|\psi(t)\rangle = \sum_q e^{-iE_q t/\hbar}\langle g;1_m|E_q\rangle\langle E_q|e;0\rangle. \tag{22b}$$

The evaluation of these equations for $c(t)$ and $b_m(t)$ begins with the calculation of the classical frequencies and mode functions for the modes that are near resonance with the atomic transition frequency. These quantities are used to generate a matrix representation of the multimode quantum Hamiltonian, and this Hamiltonian is diagonalized numerically. The elements of the eigenvectors are the quantities $\langle e;0|E_q\rangle$ and $\langle g;1_m|E_q\rangle$ that are needed in the sums of Eqs. (22a)-(22b), and the eigenvalues give the energies E_q. The numerical calculations presented in this paper were done for systems with up to 10,000 optical modes. The Hamiltonian is large, but sparse; there is only one row with non-zero off-diagonal elements, the row with elements $\langle e;0|H_{\text{int}}|g;1_m\rangle$.

Results presented in the next section show the expected spontaneous decay of the source atom revealed in the exponential decay of $c(t)$. as well as the re-excitation of the atom when the reflected field returns to the atom. Phase effects will be revealed in the complex amplitude $c(t)$ at the time of re-excitation. Although the results presented in this paper are numerical

calculations, analytical studies of similar models have demonstrated that, in the limit of an infinitely large number of modes, the decay of the source atom is exactly exponential, and the subsequent excitations of the atom in the system are fully causal [16].

The coefficients of the basis states with excited photon modes, $b_m(t)$, can be combined to give a graphical depiction of the field propagation. The expectation value of the square of the electric field operator is

$$\langle : \hat{\mathcal{E}}^2 : \rangle = \langle \psi(t) | : \left\{ \sum_m \mathcal{E}_m(z) \left(a_m + a_m^\dagger \right) \right\}^2 : | \psi(t) \rangle, \tag{23}$$

where the colons denote normal ordering of the operators. After expanding the state vector as in Eq. (19), normally ordering the operators, and evaluating the sums, the expectation value can be written in terms of amplitudes $b_m(t)$ to find the photon in the various cavity modes:

$$\langle : \hat{\mathcal{E}}^2 : \rangle = \left| \sum_m b_m(t) \mathcal{E}_m(z) \right|^2. \tag{24}$$

The results of numerical evaluation of this formula are presented in the graphs of the following section, and show a propagating envelope that mimics many, but not all, of the properties of the classical field intensity.

5. Results

The graphs in the figures of this section display examples of the time-evolving properties of quantized systems in which single photons pass through dielectric media. Although single photons do not have an absolute phase, the graphs illustrate how information about phase accumulation and propagation speeds can be deduced.

Counter-propagating classical waves superpose to form standing waves, and the positions of the nodes and antinodes are determined by the relative phases of the counter-propagating waves. If one of the counter-propagating waves traverses a region of negative-index media, this will affect the relative phase, and thus the position of the standing wave. In this example, I use Eq. (24) to calculate the quantum intensity expectation value in the region where a photon "overlaps with itself" after reflection from an end wall of the cavity. This quantum intensity exhibits a standing-wave pattern that is analogous to the standing waves observed in classical waves. I demonstrate that the insertion of a thin region of negative-index media causes the quantum pattern to shift in the same way predicted for classical waves propagating through negative-index media.

I also investigate the effect of the reflected photon on the emitting atom. Again, the photon does not have an absolute phase, but evidence of negative phase accumulation is discernible in the complex re-excitation amplitude of the emitting atom.

5.1. *Example I*

The calculations in this section were performed for the model system of Fig. 1, with the atom located at position $z_a = 0.40L$, and a narrow dielectric region of width $d = 0.0160L$ (corresponding to $12,000\lambda_{\text{medium}}$) positioned adjacent to the right end mirror. The constants characterizing the medium in this section are chosen so that $\epsilon(\omega) = \mu(\omega) = -3/2$. The equality of ϵ and μ makes the impedance of the material equal to the impedance of the vacuum, eliminating reflection at the vacuum-material interfaces, and thereby simplifying interpretation of the results presented in this section. The magnitude of the phase velocity in a medium with these properties is $2c/3$.

M. Ligare
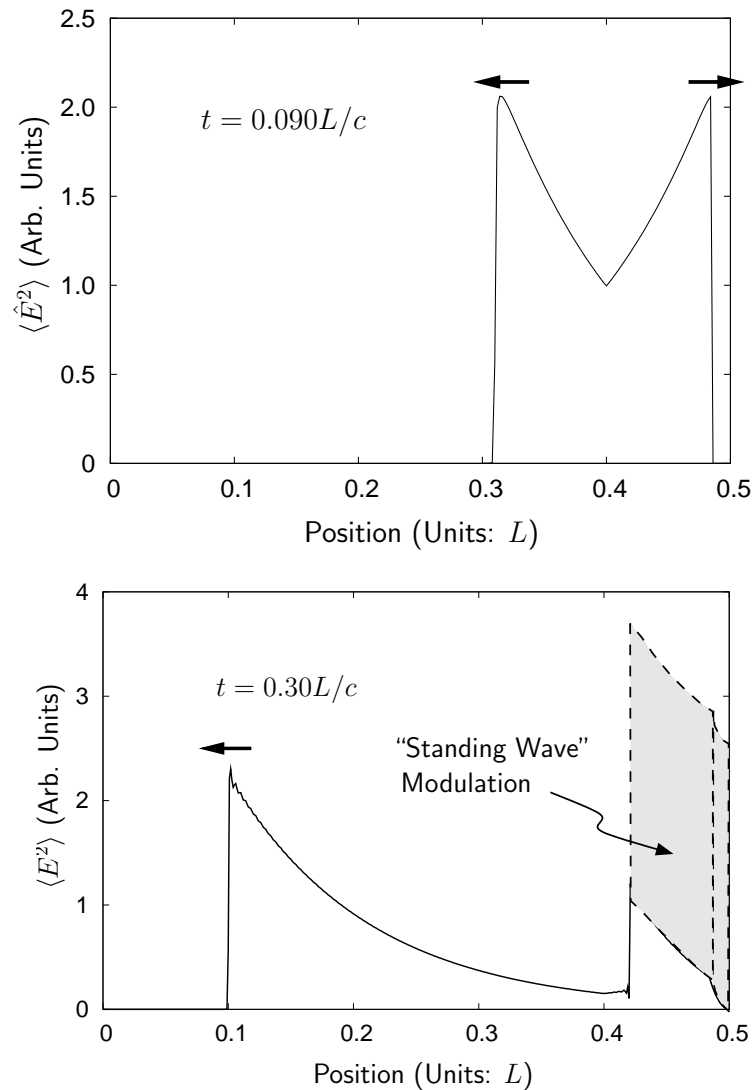
Figure 2. Evolution of expectation value of field intensity. The top graph shows the intensity at $t = 0.09L/c$ as left- and right-traveling pulses propagate away from the atom located at $z_a = 0.4L$. The smooth envelope shows no modulation on the scale of an optical wavelength. The lower graph shows the intensity at $t = 0.3L/c$ after the right-traveling pulse has propagated through the dielectric and has reflected back upon itself. Standing wave modulation on the scale of an optical wavelength occurs in the shaded regions to the right of $z = 0.42L$ in the region where left and right-traveling fields overlap. The spatial modulation is on too fine a scale to be seen in this figure; a small section of the standing wave region is displayed with an expanded scale in Fig. 3.

The dispersive characteristics of the medium were chosen so that the magnitude of the group velocity is $4c/19$. (The material constants are summarized in Table 1.) All calculations are done for systems in which the resonant frequency of the atom is $\omega = \pi \times 10^6 c/L$, or equivalently $\lambda = 2 \times 10^{-6}L$, and they include up to 10,000 optical modes.

Figure 2 shows the intensity expectation value at two times. At time $t = 0.09L/c$ the field is propagating away from the spontaneously emitting source atom to both the left and the right, and it exhibits smooth exponential spatial envelopes that reflect the temporal exponential decay of the emitting atom. The intensity expectation value does not exhibit the modulation on the scale of an optical wavelength that would be expected for a classical field — this is a manifestation of the fact that the single-photon quantum field does not have an absolute phase. (Similar graphs are displayed in [14] and [15].) At $t = 0.09L/c$ the leading edge of the left-traveling pulse is at $z = 0.31L$, and the right-traveling pulse is at the threshold of the dielectric region. The envelopes
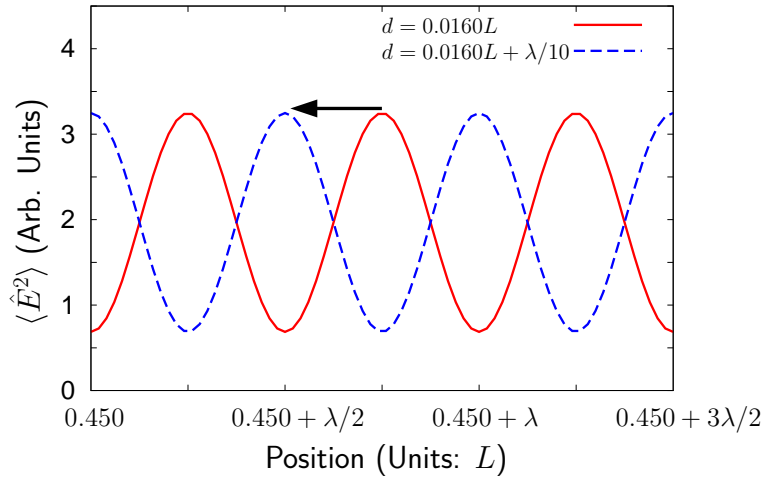
Figure 3. Standing wave intensity in the overlap region at time $t = 0.3L/c$ for the model of Fig. 1. When the dielectric region with negative index has a width $d = 0.0160L$ there is an antinode at the position of the base of the illustrated arrow. An increase in the width of the dielectric region by $\lambda/10$ results in the antinode shifting to the left by $\lambda/4$.

match the analytical expression for the expectation value [16]; for example the right-traveling envelope is given by

$$\langle \hat{E}(x)^2 \rangle = E_0^2 \exp[2\gamma(x - ct - 0.4L)/c], \qquad (25)$$

where γ is the spontaneous decay rate determined by the magnitude of the dipole matrix element of the atomic transmission.

At the later time $t = 0.3L/c$, the left-traveling pulse has propagated to $z = 0.1L$, while the leading edge of the right-traveling pulse has passed through the dielectric, reflected from the mirror, and has emerged from the dielectric traveling to the left, and has reached $z = 0.42L$. The position of the wavefront is consistent with the reduction of the group velocity within the dielectric to $4c/19$, as is predicted by classically by Eq. (6). In the region to the right of $z = 0.42$, the left-traveling reflection overlaps with the tail of the field that is still traveling to the right. In this region of overlap the photon "interferes with itself" and the intensity expectation value exhibits a standing-wave-like modulation. The modulation occurs on the scale of an optical wavelength, which is too small to be directly visible in the lower graph of Fig. 2. A small section of the standing-wave region in the neighborhood of $z = 0.45L$ is illustrated with an expanded scale in Fig. 3. The pattern of this graph is exactly what is expected for the envelope of classical standing waves. The modulation is not complete because the overlapping fields do not have equal amplitudes, and the quantum pattern is completely consistent with the standing-wave ratio calculated using the classical reflection coefficient. (In contrast to the classical pattern, the quantum standing-wave pattern does not oscillate in time at the optical frequency.) The modulation of the intensity in the region of overlap is in sharp contrast to the smooth nature of the intensity expectation value (on the scale of a wavelength) in other regions. This is a manifestation of the fact that although the one-photon field does not have an absolute phase, it does have a phase "relative to itself" [14, 15].

Information about the phase accumulated in traversing the dielectric medium is revealed in the position of the standing-wave envelope of the quantum field intensity. Antinodes of the standing wave pattern of Fig. 3 are the quantum manifestation of a classical optical path length from the position of the antinode to the end wall and back that corresponds to a phase accumulation that is an integer multiple of 2π. If the length of the dielectric region is increased by an amount Δd, the classical round-trip optical path length is increased by an amount $2(n-1)\Delta d$, and this
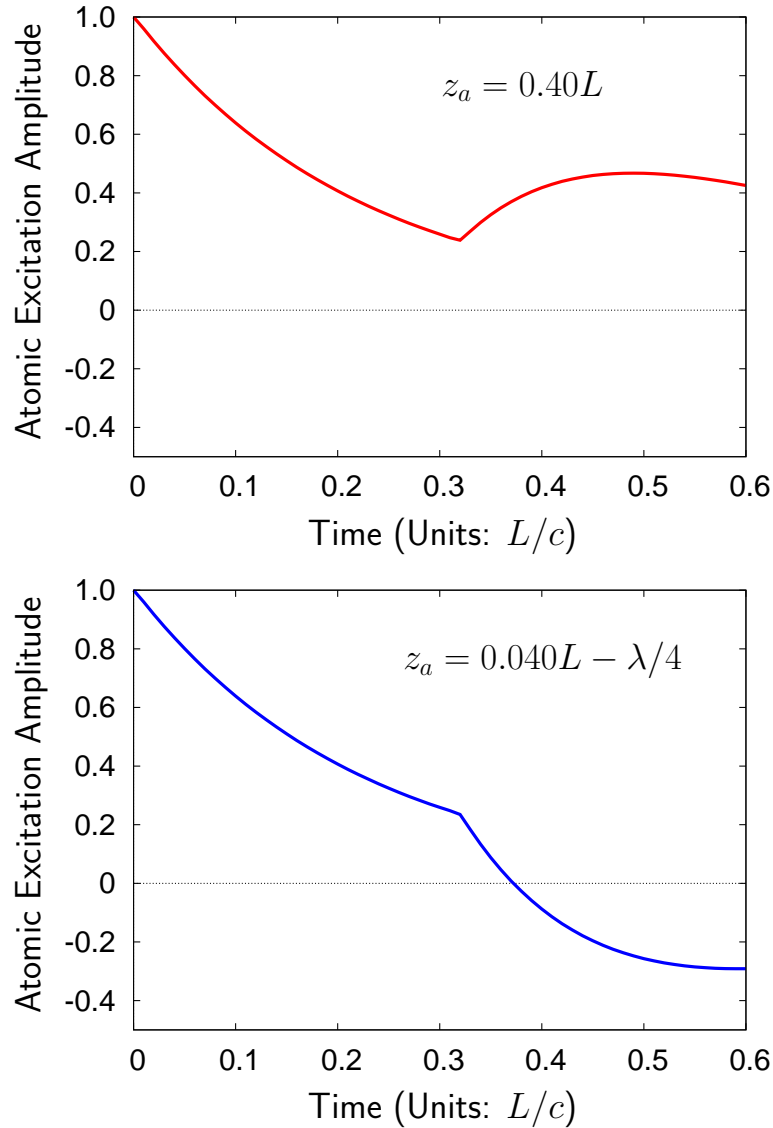
Figure 4. Atomic excitation amplitudes for model illustrated in Fig. 1 The dielectric thickness is $d = 0.0160L = 12,000\lambda_{\mathrm{material}}$ in both graphs. In the bottom graph the atom has been moved to the left by $\lambda/4$, adding extra optical path length between the atom and the reflecting wall.

leads to shift in the position of the classical standing wave pattern by an amount

$$\Delta z_{\mathrm{node}} = (n-1)\Delta d. \tag{26}$$

For a medium with an index of refraction $n > 1$, the pattern shifts to the right; for the medium considered in this section with $\epsilon = \mu = -3/2$, and $n = -3/2$, the classical wave pattern shifts *to the left* by an amount $-5\Delta d/2$. The dashed-line graph in Fig. 3 shows the results of the quantum calculations when the width of the dielectric region is increased from $d = 0.0160L$ to $0.0160L + \lambda/10$. The standing wave pattern shifts to the left by $\lambda/4$ in a manner completely consistent with classical expectations.

A second way to illustrate phase effects in the quantum system is to observe the effect of the reflected wave on the emitting atom. The atomic excitation amplitude, $c(t)$, is plotted in the top graph of Fig. 4. The atom exhibits exponential spontaneous decay, which is interrupted at time

$t = 0.32L/c$ when the first reflection returns to the position of the source, and acts to re-excite the atom. It is worth noting that the exponential decay, as well as the abrupt change due to re-excitation by the reflected photon, both emerge from the evaluation of the single formula given in Eq. (22a). All the information about the material properties and the positions of the boundaries is encoded in the value of the mode functions at the positions of the atom. (The amplitude c is in general complex; I have chosen conditions under which it is purely real.)

The effect of a reflection on the source atom depends, in general, on the optical path length to the reflecting surface [13–15]. This is illustrated in the bottom graph of Fig. 4, with a plot of the excitation amplitude when the atom is moved one-quarter wavelength farther away from the right end wall, i.e., $z_a \longrightarrow 0.40 - \lambda/4$. In this case the reflection acts to *reduce* the excitation amplitude, $c(t)$. This is the quantum manifestation of the fact that a classical reflected wave will return to the atom at $z_a = 0.40L - \lambda/4$ with a phase lag of π when compared to the case with the atom at $0.40L$, and a classical wave can either add energy to a dipole oscillator, or remove it, depending on the relative phase of the field and the oscillator.

In general, after the reflection arrives, the complex quantum amplitude for the source to be excited can be written as

$$c(t) = e^{-\gamma t} + e^{i\delta}c_{\text{refl}}(t), \tag{27}$$

where δ is the classical phase accumulated on the path to the reflecting surface and back, and $c_{\text{refl}}(t)$ is a real function giving the amplitude for excitation due to the reflected field. The function $c_{\text{refl}}(t)$ depends on the nature of the reflecting surface, but not the optical path length to the surface. If, in the previous example, the atom is moved to the left by $\lambda/8$ (instead of $\lambda/4$), the phase factor $e^{i\delta}$ becomes pure imaginary.

The algebraic sign of the phase accumulation in the dielectric region can be demonstrated by changing the position of the source atom, and determining the change in the thickness of the dielectric that will exactly compensate for the increased optical path length due to the change in the position of the atom. If this is accomplished, the excitation amplitude $c(t)$ will return to its original form. A simple calculation shows that if the atom is moved to the left a distance Δz_a, the classical optical path length to the right wall and back is unchanged if the thickness of the dielectric is decreased by an amount

$$\Delta d = \frac{\Delta z_a}{(n-1)}. \tag{28}$$

In the case under consideration here, with $n = -3/2$, the quantity Δd is negative, indicating that the length of the dielectric region must actually be *increased* in order to compensate for the extra path length. Repeating the numerical calculation of the atomic excitation amplitude with $z_a = 0.40L - \lambda/4$ and $d = 0.0160L + \lambda/10$ reproduces the top graph in Fig. 4, indicating that the classical phase δ in the exponent of the complex quantum phase factor has returned to its original value.

5.2.   *Example II*

In the preceding section the material properties were chosen such that $\epsilon = \mu$, leading to a reflectionless vacuum-dielectric interface. For completeness, I show in Fig. 5 the results for an example in which this is not the case. In this example $\epsilon = -3$, $\mu = -4/3$, and $v_{\text{gr}} = 5c/27$ (see Table 1). The atom is at the same position as in the previous example ($z = 0.4L$) and again the dielectric material is located to the right of $z = 0.484$. The figure shows the expected agreement with classical predictions. At time $t = 0.13L/c$ the leading edge of the pulse in the dielectric is at 0.493, which is consistent with propagation at the classical group velocity, and the intensity
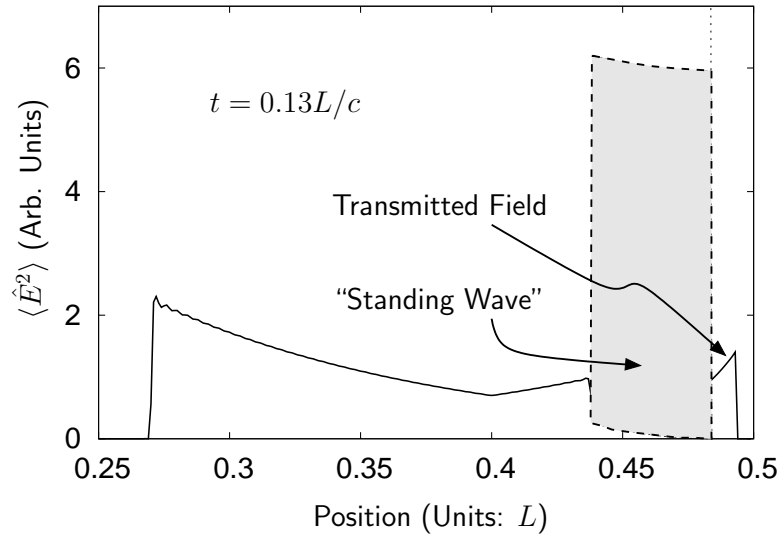
Figure 5.   Expectation value of field intensity for model with reflection at vacuum-dielectric interface. The source atom is locate at $z = 0.4L$ and the dielectric is located to the right of the dotted line at $z = 0.484L$. (Material properties are listed in Table 1.) The transmitted field within the dielectric is reduced by the classical transmission coefficient and propagates at the classical group velocity. Standing wave character is present in the region immediately to the left of the vacuum-dielectric interface where the reflected field overlaps with the right-traveling field from the source.

has been reduced by the classical transmission coefficient $[2/(1 + \sqrt{\epsilon/\mu})]^2 = 16/25$. Standing wave character is again evident in the region immediately to the left of the interface where left- and right-traveling fields overlap.

6.   Conclusions

Although the striking optical properties of negative-index media can be described in terms of classical physics, it is still instructive to investigate the quantum analogs of the classical properties. I have demonstrated a model of a multimode single-photon field with features that make the comparison between the classical and quantum descriptions straightforward. The spatially localized energy density of the photon field in this model has well-defined wavefronts that travel at the classical group velocity. The classical phase velocity is not as apparent in the quantum model, because the photon field has no absolute phase, but interference effects in the quantum model illustrate close analogs to the accumulation of negative phase by classical fields when light propagates through negative-index materials.

References

[1]   Veselago, V.G. The Electrodynamics of Substances with Simultaneously Negative Values of ϵ and μ. *Sov. Phys. Usp.* **1968**, *10*, 509–514. originally published in Russian in Usp. Fiz. Nauk., **92**, 517-526 (1967).
[2]   Pendry, J.B. Negative Refraction Makes a Perfect Lens. *Phys. Rev. Lett.* **2000**, *85*, 3966–3969.
[3]   Pendry, J.B. Negative Refraction. *Cont. Phys.* **2004**, *45*, 191–202.
[4]   Ramakrishna, S.A. Physics of negative refractive index materials. *Rep. Prog. Phys.* **2005**, *68*, 449–521.
[5]   Shalaev, V.M. Optical negative-index metamaterials. *Nature Photonics* **2007**, *1*, 41–48.
[6]   McCall, M.W. What is negative refraction. *J. Mod. Opt.* **2009**, *56*, 1727–1747.
[7]   Cai, W.; Shalaev, V. Optical Metamaterials: Fundamentals and Applications. Springer: New York, 2009.
[8]   Cui, T.J.; Smith, D.; Liu, R. (Eds.), Metamaterials: Theory, Design, and Applications. Springer: New York, 2009.
[9]   Peřinová, V.; Lukš, A.; Peřina, J., 4, *Phase in Optics* ; World Scientific, Singapore, 1982; and references therein.
[10] Orszag, M., 15, *Quantum Optics* ; Springer-Verlag, Berlin, 2000; and references therein.
[11] Landau, L.D.; Lifshitz, E.M. Electrodynamics of Continuous Media. Pergamaon Press: Oxford, 1960.

[12] Ligare, M.; Becker, S.F. Simple soluble models of quantum damping applied to cavity quantum electrodynamics. *Am. J. Phys.* **1995**, *63*, 788–796.

[13] Gießen, H.; Berger, J.D.; Mohs, G.; Meystre, P.; et al. Cavity-modified spontaneous emission: From Rabi oscillations to exponential decay. *Phys. Rev. A* **1996**, *53*, 2816–2821.

[14] Bužek, V.; Drobný, G.; Kim, M.G.; Havukainen, M.; et al. Numerical simulations of atomic decay in cavities and material media. *Phys. Rev. A* **1999**, *60*, 582–592.

[15] Ligare, M.; Oliveri, R. The calculated photon: Visualization of a quantum field. *Am. J. Phys.* **2002**, *70*, 58–66.

[16] Purdy, T.; Taylor, D.F.; Ligare, M. Manifestation of classical wave delays in a fully-quantized model of the scattering of a single photon. *J. Opt. B: Semiclass. Quantum Opt.* **2003**, *5*, 85–91.

[17] Purdy, T.; Ligare, M. Electromagnetically induced transparency and reduced speeds for single photons in a fully quantized model. *J. Opt. B: Semiclass. Quantum Opt.* **2003**, *5*, 289–299.

[18] Milonni, P.W.; Maclay, G.J. Quantized-field description of light in negative-index media. *Opt. Comm.* **2003**, *278*, 161–165.

[19] Milonni, P.W. Field quantization and radiative processes in dispersive dielectric media. *J. Mod. Optics* **1995**, *42*, 1991–2004.

[20] Knöll, L.; Vogel, W.; Welsch, D.G. Action of passive, lossless optical systems in quantum optics. *Phys. Rev. A* **1987**, *36*, 3803–3818.

[21] Glauber, R.J.; Lewenstein, M. Quantum optics of dielectric media. *Phys. Rev. A* **1991**, *43*, 467–491.

[22] Santos, D.J.; Loudon, R. Electromagnetic-field quantization in inhomogeneous and dispersive one-dimensional systems. *Phys. Rev. A* **1995**, *52*, 1538–1549.

[23] Dung, H.T.; Buhmann, S.Y.; Knöll, L.; Welsch, D.G.; Scheel, S.; et al. Electromagnetic-field quantization and spontaneous decay in left-handed media. *Phys. Rev. A* **2003**, *68*, 043816.

[24] Kästel, J.; Fleischauer, M. Quantum Electrodynamics in Media with Negative Refraction. *Laser. Phys.* **2005**, *15*, 135–145.

[25] Philbin, T.G. Canonical quantization of macroscopic electromagnetism. *New J. Physics* **2010**, *12*, 123008.

[26] Knöll, L.; Scheel, S.; Welsch, D.G. QED in dispersing and absorbing media. In *Coherence and Statistics of Photons and Atoms*; Peřina, J. Ed.; Wiley: New York, 2001; pp 1–63.

[27] Scheel, S.; Buhmann, S.Y. Macroscopic quantum electrodynamics — concepts and applications. *Acta Physica Solvaca* **2008**, *58*, 675–809.

[28] Meystre, P.; Sargent, M. Elements of Quantum Optics.2nd; Springer: Berlin, 1991.

[29] Sargent, M.; Scully, M.O.; Lamb, W.E. Laser Physics. Addison-Wesley: Reading, MA, 1974.

[30] Loudon, R. The Quantum Theory of Light.2nd; Oxford U. P.: Oxford, 1983.

Appendix A. Classical Normal Mode Calculations

The field quantization scheme used in this paper starts with the determination of the classical normal modes of the field in the entire volume. As an example, consider the model illustrated in Fig. 1. The mode functions have the form

$$\mathcal{E}_m = A_m \begin{cases} \sin\left[k_m^{\text{vac}}(z + L/2)\right] & \text{for } -L/2 \leq z < L/2 - d \\ B_m \sin\left[\sqrt{\epsilon(\omega_m)\mu(\omega_m)}\, k_m^{\text{vac}}(z - L/2)\right] & \text{for } L/2 - d \leq z \leq L/2 \end{cases} . \tag{A1}$$

The boundary conditions at $z = d$ are automatically satisfied by the functional form that was chosen for these expressions. Application of the standard boundary conditions at the vacuum-dielectric interface at $z = d$ gives the condition

$$\sin\left(\sqrt{\epsilon\mu}\, k^{\text{vac}}d\right)\cos\left[k^{\text{vac}}(L - d)\right] + \frac{\sqrt{\epsilon\mu}}{\mu}\cos\left(\sqrt{\epsilon\mu}\, k_m^{\text{vac}}d\right)\sin\left[k_m^{\text{vac}}(L - d)\right] = 0, \tag{A2}$$

as well as an expression for the relative field amplitude in the dielectric,

$$B_m = \frac{\sin\left[k_m^{\text{vac}}(L - d)\right]}{\sin\left[\sqrt{\epsilon\mu}\, k_m^{\text{vac}}d\right]}. \tag{A3}$$

Numerical solution of Eq. (A2) gives a set of possible vacuum wave-numbers k_m^{vac}, and these can then be used in Eq. (A3) to determine the relative field amplitudes of the modes in the dielectric. The constants A_m are determined by the normalization condition that the integrated energy density in a mode must be equal to $\hbar\omega_m$.